UNIVERSITY OF CALIFORNIA

Santa Barbara

Quantifying and Understanding Voltage Losses Due to Nonradiative Recombination in Bulk Heterojunction Organic Solar Cells with Low Energetic Offsets

A Thesis submitted in partial satisfaction of the

requirements for the degree Master of Science

in Chemistry

by

Katie Danielle Rosenthal

Committee in charge:

Professor Thuc-Quyen Nguyen, Chair

Professor Martin Moskovits

Professor Mattanjah S. de Vries

June 2019

The thesis of Katie Danielle Rosenthal is approved.

_____
Thuc-Quyen Nguyen, Committee Chair

_____
Mattanjah S. de Vries

_____
Martin Moskovits

March 2019

Quantifying and Understanding Voltage Losses Due to Nonradiative Recombination in Bulk Heterojunction Organic Solar Cells with Low Energetic Offsets

by

Katie Danielle Rosenthal

ACKNOWLEDGEMENTS

Ms. Katie Danielle Rosenthal would like to acknowledge the following people for their significant contribution to the completion of this work. Firstly, I would like to thank my mother, father and stepfather for their love, support and encouragement throughout my life, establishing a foundation from which I was able to accomplish my educational goals. Secondly, I would like to thank Professor Gail Tang and Professor Iraj Parchamazad from my undergraduate institution, University of La Verne, for their advice and guidance as I navigated my decision to attend graduate school. At the University of California, Santa Barbara, I would like to thank Professor Nguyen for the opportunity to conduct this work, Professor Martin Moskovits for giving me the courage to complete this work, and Professor Mattanjah de Vries for the confidence to believe that I deserve to complete this work. Finally, I'd like to thank my family, Michael and Lily Hughes, for being the primary source of joy, laughter, love and encouragement throughout my graduate career, without which I never could have finished.

ABSTRACT

Quantifying and Understanding Voltage Losses Due to Nonradiative Recombination in Bulk Heterojunction Organic Solar Cells with Low Energetic Offsets

by

Katie Danielle Rosenthal

Open-circuit voltage (V_{OC}) losses in organic photovoltaics (OPVs) inhibit devices from reaching V_{OC} values comparable to the bandgap of the donor-acceptor blend. Specifically, nonradiative recombination losses (ΔV_{nr}) are much greater in OPVs than in silicon or perovskite solar cells, yet the origins of this are not fully understood. To understand what makes a system have high or low loss, an investigation of the nonradiative recombination losses in a total of nine blend systems was carried out. An apparent relationship was observed between the relative domain purity of six blends and the degree of nonradiative recombination loss, where films exhibiting relatively less pure domains show lower ΔV_{nr} than films with higher domain purity. Additionally, it is shown that when paired with a fullerene acceptor, polymer donors which have bulky backbone units to inhibit close π-π stacking exhibit lower nonradiative recombination losses than in blends where the polymer can pack more closely. This work reports a strategy that ensures ΔV_{nr} can be measured accurately and reports key observations on the relationship between ΔV_{nr} and properties of the donor/acceptor interface.

TABLE OF CONTENTS

I. Introduction

Organic photovoltaic cells (OPVs) allow for lightweight, flexible, and semitransparent energy generation, permitting them to be used for such unique purposes as building-integrated applications.[1–3] Significant improvements in materials design and processing and the development of nonfullerene acceptors have allowed for near constant reports of record-breaking efficiency in these devices over the past 30 years;[4–6] some systems now achieve fill factors (FF) near 80%[7] and others show external quantum efficiencies (EQE) of over 80%.[8] However, all of these devices remain plagued by large open-circuit voltage (V_{OC}) losses. The optimal bandgap for OPVs has been reported to be between 1.45 eV and 1.65 eV,[9] but due to the high recombination-based losses, open-circuit voltages above 1.0 V are rarely observed.[10] In fact, a well-established empirical relationship has been reported: $qV_{OC} = E_{CT} - 0.6$ eV, where 0.6 eV accounts for both radiative and nonradiative recombination losses. Because the short-circuit current (J_{SC}) and FF of some OPV devices are already nearing a theoretical limit, further improvements in OPV PCEs will depend on mitigating voltage losses.

The maximum theoretical V_{OC} of an OPV device is dictated by the device's optical gap (E_{opt}), which is defined as the transition energy between the ground state, S_0, and the lowest energy excited state, S_1, of either the donor or the acceptor material ($S_0 \rightarrow S_1$).[11] After photoexcitation, the bound electron-hole pair, termed exciton, migrates to the donor/acceptor interface where electron-transfer losses occur as a result of the exciton relaxing into a delocalized charge transfer (CT) state ($S_1 \rightarrow E_{CT}$). Several recent results suggest that there are systems with energy offsets less than 50 meV between the donor E_{opt} and E_{CT} which still exhibit efficient charge separation at the donor/acceptor interface,[12,13] reinforcing the notion that the greatest opportunity for increasing V_{OC} lies in mitigating recombination-based losses.

Equation 1[14,15] relates recombination-based open-circuit voltage losses to the CT state,

$$V_{OC} = \frac{E_{CT}}{q} - \Delta V_{rad} - \Delta V_{nr} \quad (1)$$

In which the first term includes $E_{CT,}$ the energy of the CT state, and the second and third terms account for the magnitude of recombination losses via radiative and nonradiative pathways, respectively. Radiative recombination loss, ΔV_{rad}, ranges narrowly in value from 200 – 250 meV and is ultimately unavoidable due to the equilibrium between absorption and emission processes.[16] Contrastingly, the magnitude of nonradiative recombination losses, ΔV_{nr}, has been reported to span a much larger range of 250-550 meV.[9] The reason for this wide range is still poorly understood, and more research is needed to better understand the origins and controllability of nonradiative recombination losses.

The study of nonradiative recombination losses in OPVs has only recently become a popular topic of study, with several experimental-[17–21] and theory- based[22,23] studies being published in the past three years. Recent research suggests that nonradiative recombination may be attributed to carbon-carbon bond vibrations, implying that the very molecular nature of OPVs lead to high recombination based losses.[9] Other studies have found a strong relationship between molecular orientation at the donor/acceptor interface and the degree of nonradiative recombination loss, such that a system where the donor is oriented primarily edge-on to the acceptor has higher ΔV_{nr} than the same system with the donor positioned predominantly face-on to the acceptor.[17,22] Nonradiative recombination losses have been shown to roughly correlate with the energy of the charge transfer state E_{CT}, where systems with higher E_{CT}, in general, show lower ΔV_{nr} than systems with low E_{CT}.[9] Because the nonradiative decay takes place between the lowest energy CT state and the ground state, the

energy of this state is expected to be relevant to this question. However, the large range of ΔV_{nr} at a constant E_{CT} indicates other factors such as the energetic driving force,[21] molecular weight,[18] isotopic substitution,[23] and device processing[20] may also be involved. Nevertheless, our current understanding is insufficient to successfully inform optimal synthetic strategies for producing low ΔV_{nr} materials.

Also absent from the literature is a clear consensus on how to accurately measure ΔV_{nr}. The methods to do so are based on assumptions which were evaluated for feasibility at their inception but have not been reevaluated for newer, more efficient systems, particularly systems with low offsets between E_{opt} and E_{CT}. Two of the three ways most frequently used to determine recombination-based losses in OPVs are based on a spectral measurement of the absorption shoulder of the CT state, which can be difficult to identify using even high sensitivity measurements such as Fourier-transform photocurrent spectroscopy (FTPS) and becomes increasingly difficult when the weakly-absorbing CT state absorbs at the same energy as the strongly-absorbing singlet state of the donor or acceptor. A recently published communication explained how to measure electron-transfer and recombination-based voltage losses most accurately;[11] my current work adds to that strategy by delving deeply into the three main methods for measuring ΔV_{nr} specifically, and how these methods compare in systems with low offset between E_{opt} and E_{CT}.

This study is both an investigation of the methods used to measure nonradiative voltage losses in OPVs as well as an in-depth analysis of the data collected on nine material systems. My analysis centers around the theory that the donor/acceptor interface and strength of donor-acceptor coupling play the largest roles in the observed difference in magnitude of nonradiative voltage losses among systems. I was able to probe this theory using different

material combinations and processing conditions so as to identify "high loss" and "low loss" factors in our systems. I observed a clear relationship between domain purity and ΔV_{nr} in a cross-system comparison but also saw that altering processing conditions on a single system showed a minimal impact on this value. Moreover, I suggest a link between steric inhibition and lower nonradiative recombination losses.

II. Results and Discussion

A. Methodology for determining the magnitude of voltage losses

As it becomes increasingly relevant to understand factors which dictate the magnitude of voltage losses in a given OPV system, a priority should be that the OPV community collects and analyzes experimental results uniformly. In the following section, I will discuss three methods most commonly referenced in the literature to measure the magnitude of nonradiative and radiative loss in OPVs. I describe their methodology, address the assumptions which are made in each case and investigate cases where these assumptions may fail.

1. EQE_{EL} measurement

The ΔV_{nr} of a device is most directly measured experimentally by determining its radiative efficiency, termed the electroluminescence external quantum efficiency (EQE_{EL}).[14,24] The EQE_{EL} is defined as the ratio of photons emitted from the device per electrons injected into the device, which can be obtained by applying a small bias across the OPV device and measuring the resulting luminescent output with a photodiode. The ΔV_{nr} can be found from the EQE_{EL} using the following well-established relationship, in which k_B is Boltzmann's constant and T is temperature:

$$\Delta V_{nr}(T) = \frac{k_B T}{q} \ln\left(\frac{1}{EQE_{EL}}\right) \quad (2)$$

While this method can be a relatively simple and robust way to determine the nonradiative voltage loss of a system, a few key factors should be considered. First, it is important to evaluate the ΔV_{nr} at a bias which corresponds to an injected current equivalent to the magnitude of the J_{SC} of the device under 1 sun illumination, a bias which I will refer to as V_{Jsc}. This ensures that the ΔV_{nr} obtained is the relevant value under simulated operating conditions of the device; using a larger bias can result in a higher determined radiative efficiency due to the abnormally high charge carrier density and potential deviation from quasi-equilibrium conditions.[11] I explore various points of evaluation in **Figure S3**, where I find that evaluating the EQE_{EL} at a bias corresponding to the V_{OC} of the device at 1 sun conditions shows little variation (<20 meV) from the bias corresponding to V_{Jsc}, but do confirm that when voltages much beyond V_{Jsc} are used to evaluate ΔV_{nr}, the increased charge carrier density in the device will artificially lower the measured value of ΔV_{nr}.

Also, because of the low radiative efficiency of these devices (10^{-3}–10^{-6} percent), the signal received by the photodiode is often only tens of nA, meaning these measurements must be taken in extremely dark conditions to minimize background signal. Even so, systems with EQE_{EL} below 10^{-5} percent may not be luminescent enough for voltage loss determination using this method. Finally, to determine the number of photons emitted from the device, the current output from the photodiode should be multiplied by a factor which accounts for the electroluminescence spectra of the device, details of which can be found in the Appendix.

When all of these conditions are met, this approach becomes a good strategy for measuring ΔV_{nr}. One other important consideration that needs to be kept in mind when using this technique is that it assumes that charge recombination occurs through bimolecular

processes, and, as a result, the ΔV_{nr} of systems affected by high levels of Shockley-Read-Hall (deep trap) recombination at high carrier densities cannot be quantified using such measurements. Systems which have high levels of trapping show a high voltage dependence in the $EQE_{EL}(V)$ spectra in the range from below V_{Jsc} to 2 V due to the filling of trap states,[25,26] and as a result, the value of EQE_{EL} becomes ambiguous. For this reason, I suggest that the voltage dependence of the EQE_{EL} should always be evaluated before trusting ΔV_{nr} values obtained in this way.

Each system reported in this paper was measured in this manner, and values for ΔV_{nr} reported are averages over at least 20 devices taken from multiple device batches. In most cases the device-to-device ΔV_{nr} values for nominally equivalent devices were reproducible within <10 meV, and even these small variations can typically be accounted for by differences in device leakage current (Figure S3**)**. In an attempt to further test this method's robustness, I varied the distance between the photodiode and the emitting BHJ solar cell device from ~4cm to <1cm and found that 96% of the photons collected in the "close" distance measurement (**Figure S4)** are already measured at the "far" distance.

Overall, my assessment of this method reveals that the EQE_{EL} measurement is quite robust if done correctly, and can also provide other useful information, such as the presence of deep-traps and the magnitude of radiative loss, if the E_{CT} of the device is known. Additionally, the ΔV_{nr} determined in this way is independent of the measured V_{OC}, unlike the other two methods I will discuss, making the EQE_{EL} measurement a viable check for the calculation-based methods.

2. Calculating ΔV_{nr} from the EQE_{PV} spectra

The magnitude of nonradiative recombination losses can also be calculated from J-V and photovoltaic external quantum efficiency (EQE_{PV}) measurements. This method is derived from the intrinsic reciprocity between absorption and emission, which can inform us of the radiative limit to the open-circuit voltage, $V_{OC,rad}$.[14,27] $V_{OC,rad}$ represents the maximum V_{OC} achievable in the absence of nonradiative recombination, when only recombination loss from radiative pathways is considered. Due to the principle of detailed balance, it is understood that any light absorption process must be accompanied by some amount of light emission. Based on this, the same principles used to define V_{OC} can be used to define $V_{OC,rad}$.[14,27] V_{OC} is defined as

$$V_{OC} = \frac{nk_BT}{q} ln\left(\frac{J_{ph}(V_{OC})}{J_0} + 1\right) \quad (3)$$

where n is the ideality factor, k_B is Boltzmann's constant and $J_{ph}(V_{OC})$ is the photocurrent at V_{OC}.[27] In the limit of only radiative recombination, n=1, $J_0 = J_{0,rad}$ and $J_{ph}(V_{OC,rad}) \approx J_{SC}$, which, together with **Equation 3** produces the following:

$$V_{OC,rad} = \frac{k_BT}{q} ln\left(\frac{J_{SC}}{J_{0,rad}} + 1\right) \quad (4)$$

where $J_{0,rad}$ represents the current density simulating the device's blackbody radiation at room temperature. This term is calculated by integrating the product of $EQE_{PV}(E)$ and the black body emission spectra at room temperature, , $\phi_{BB}(E)$ over energy:

$$J_{0,rad} = q\int_0^\infty EQE_{PV}(E)\phi_{BB}(E)dE \quad (5)$$

For an OPV device , ϕ_{BB} can be approximated by

$$\phi_{BB}(T) = \frac{2\pi}{h^3c^2}E^2 \exp\left(-\frac{E}{k_BT}\right) \quad (6)$$

where T=300K.[19] Note that the definition of $J_{0,rad}$ given in **Equation 5** is similar to the definition of J_{SC} when $\phi_{BB}(E)$ is replaced with the solar flux density, $\phi_{sun}(E)$

$$J_{SC} = q\int_0^\infty EQE_{PV}(E)\phi_{sun}(E)dE \quad (7)$$

It follows from the definition of $V_{OC,rad}$ in **Equation 4** that the difference between $V_{OC,rad}$ and the measured V_{OC} under one sun illumination will be the voltage loss due to nonradiative recombination:

$$\Delta V_{nr} = V_{OC,rad} - V_{OC} \quad (8)$$

This method is perhaps the most frequently used in OPV literature;[9,11,18,27] however, my investigation elucidated a potential problem when this method is applied to systems in which $E_{opt} \sim E_{CT}$. **Figure 1** shows the EQE_{PV} spectra for two systems: PTB7-Th:$PC_{71}BM$, which has an offset between E_{opt} and E_{CT} of about 130 meV, and PM2:$PC_{61}BM$, where the offset is less than 50 meV. The consequence of this low offset becomes critical for one key assumption of this method, which is that the integration of the product of $\phi_{BB}(E)$ and EQE_{PV} will be dominated by charge transfer state absorption.[16] This assumption is typically valid, because at room temperature, in the relevant energy range, ϕ_{BB} exponentially increases with decreasing energy. However, in cases where $E_{opt} \sim E_{CT}$, the singlet absorption from the donor occurs at very similar energy to the charge transfer absorption.[13,20] As a result of this, the aforementioned assumption is no longer valid, and **Equation 5** will over-estimate $J_{0,rad}$, resulting in an under-estimated $V_{OC,rad}$ and a lower ΔV_{nr}. The consequence of this can be seen in **Table 1**, in which those systems with low energy offsets (PIPCP:$PC_{61}BM$ and PM2:$PC_{61}BM$) show much lower ΔV_{nr} when calculated this way than by the other two methods.

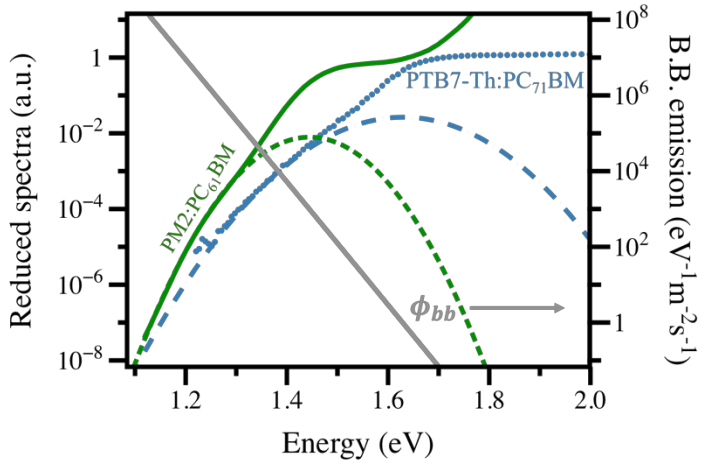

Figure 1. Reduced absorption spectra of two blends: PM2:$PC_{61}BM$ (solid green line) and PTB7-Th:$PC_{71}BM$ (blue points), which correspond to the left axis, plotted against the temperature-dependent blackbody emission spectra (gray line, corresponds to the right axis), where T=300K. The dashed lines are Gaussian fits (using Equation 9) corresponding to absorption from the charge transfer state. Any other signal from the spectra can thus be attributed to singlet absorption of the donor material itself. PM2:$PC_{61}BM$ is an example of a system with $E_g \sim E_{CT,}$ where the peak of the singlet absorption occurs at similar energy as the CT state and absorbs several orders of magnitude more strongly than the CT state, causing convolution of Equation 5, whereas PTB7-Th:$PC_{71}BM$ has sufficient offset between E_g and E_{CT} such that this method produces valid results.

3. Simultaneous fitting via Marcus Theory

The third method I discuss for determining OPV voltage losses is Marcus Theory simultaneous fitting to the measured CT state absorption and emission spectra, where the fit parameters allow for deduction of E_{CT}, ΔV_{nr} and ΔV_{rad}.[15] The fits to the charge transfer state absorption (**Equation 9**) and emission (**Equation 10**) can be described as follows:

$$EQE_{PV,CT}(E) = \frac{f}{E\sqrt{4\pi\lambda k_B T}} \exp\left(\frac{-(E_{CT}+\lambda-E)^2}{4\lambda k_B T}\right) \quad (9)$$

$$EQE_{EL,CT}(E) = E\frac{f}{\sqrt{4\pi\lambda k_B T}} \exp\left(\frac{-(E_{CT}-\lambda-E)^2}{4\lambda k_B T}\right) \quad (10)$$

in which k_B is Boltzmann's constant and T is temperature. The fit parameters are E_{CT}, which is the energy at the point of intersection between CT absorption and emission, λ, which is the reorganization energy and f, a measure of the strength of the donor-acceptor coupling. These

fit parameters, placed into the same theoretical framework as the method described in Section 2.1.2, can be used to determine ΔV_{rad} (**Equation 11**), and ΔV_{nr} can then be calculated by rearranging the relationship discussed in Equation 1.

$$\Delta V_{rad}(T) = \frac{k_B T}{q} \ln\left(\frac{f q 2\pi (E_{CT} - \lambda)}{J_{SC} h^3 c^2}\right) \quad (11)$$

The simultaneous fitting is the only method discussed here which can provide E_{CT}, ΔV_{nr} and ΔV_{rad} without any additional measurements; however, this method is not without its own caveats. The ability to precisely and uniquely identify and fit the CT spectra is of key importance to correctly determining E_{CT} as well as the resultant recombination loss values. This becomes more difficult in low energy offset systems ($E_{opt} \sim E_{CT}$), when the absorption spectrum shoulder is sharp.[12,28] **Figure 2A** shows an example of this, in which it is possible to create suitable fits across a 100 meV range for the same data. For this reason, this method should not be used to quantify energy losses for systems which show an exponential band edge.

However, it is possible to calculate the absorption down to 10^{-8} using sensitively measured electroluminescence (EL) data and the following relationship[14,29]

$$EQE_{PV}(E) \sim EQE_{EL}(E) E^{-2} \exp\left(\frac{E}{k_B T}\right) \quad (12)$$

Figure 2B illustrates the same experimentally measured EQE_{PV} spectra from Figure 2A, with the solid black line showing the calculated blend absorption from the EQE_{EL} spectra. It is clear not only that the calculated spectra align very well with experimental values, but that the added four orders of magnitude in sensitivity allows us to deconvolute the Gaussian-shaped CT absorption shoulder from the sharp singlet absorption. The clear CT shoulder allows the fit parameters to be calculated with very low error, making this method much more viable for analyzing a low energy-offset system.

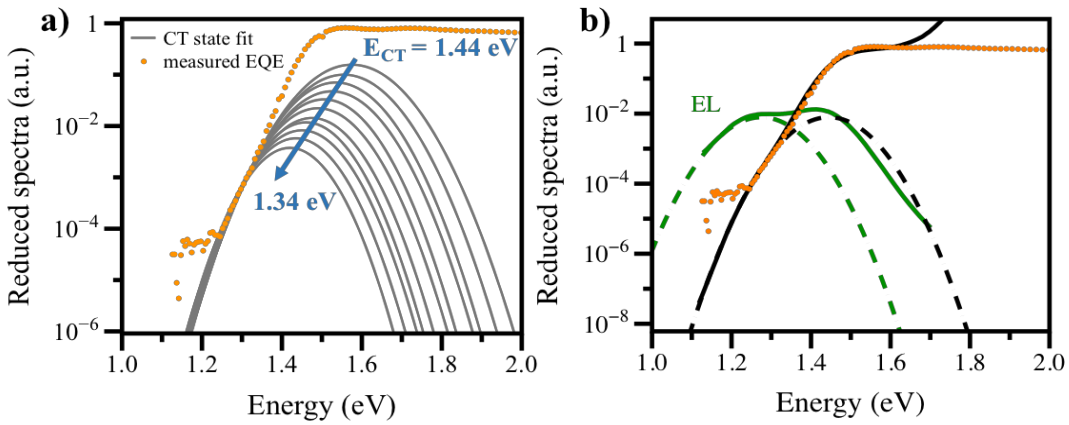

Figure 2. a) Marcus theory fitting of the EQE_{PV} of a system with low offset between E_g and E_{CT} (PM2:$PC_{61}BM$), where seemingly appropriate fits can be obtained for E_{CT} values varying over a range of 100 meV (while it is not depicted in the figure, for visual clarity, each of the fits shown also has a suitable reciprocal fit to the EL spectrum of the device). b) Simultaneous fitting of the reduced EQE_{PV} and EL spectra for the same system where the reciprocity relationship between absorption and emission has been applied to calculate the EQE_{PV} (solid black line) down to 10^{-7}. Fits (dotted lines) to the calculated EQE_{PV} spectra allow for a higher degree of certainty in determining E_{CT} (within 5 meV).

3. Methods Summary

To better understand these methodologies and explore resultant nonradiative recombination values, I chose three donor and three acceptor materials to study. The three polymer donors pictured in **Figure 3A**, PIPCP,[30] PM2[31] and PTB7-Th[32], were chosen for their systematic structural change which will be discussed in depth in Section 2.2, and for their similar highest occupied molecular orbital levels (HOMO) and dissimilar lowest unoccupied molecular orbital levels (LUMO) as seen in **Figure 3B**. My expectation was that these energy differences should provide a dissimilar E_{opt} but similar E_{CT} when blended with each electron acceptor, providing a reliable basis for comparison. The acceptors I chose were the optimal fullerene acceptor for the donor, either *[6,6]-phenyl-C61-butyric acid methyl ester* (**$PC_{61}BM$**) or *[6,6]-phenyl-C71-butyric acid methyl ester* (**$PC_{71}BM$**), and the high performing non-

fullerene acceptor **ITIC-Th**[33] to allow for comparison between fullerene- and nonfullerene-based systems. The absorption spectra of the neat materials and the optimized blends studied here are included in the Appendix for reference.

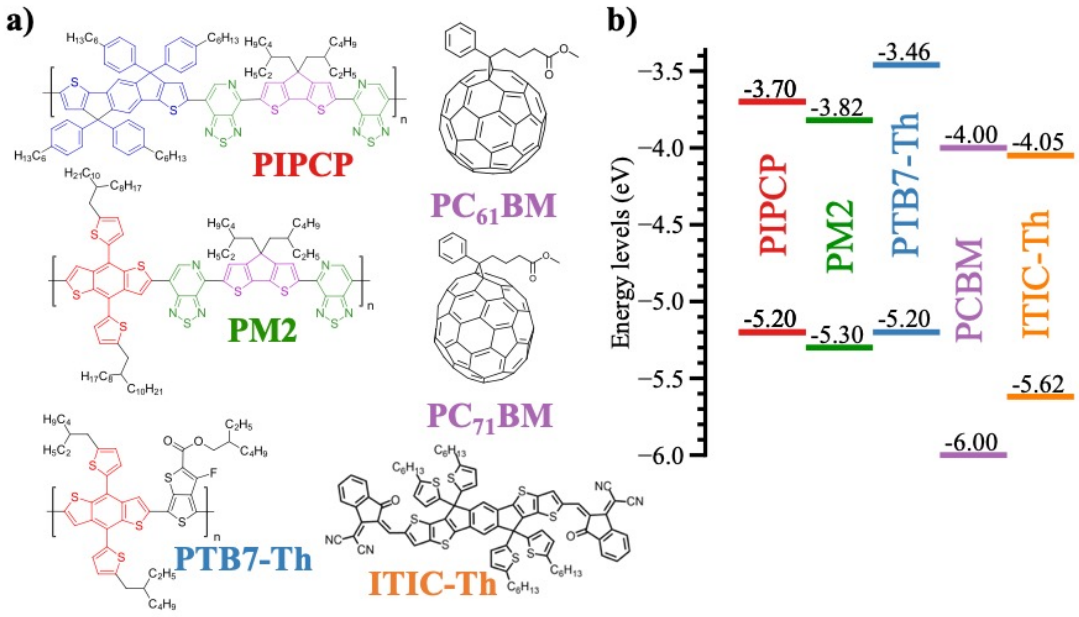

Figure 3. (a) Chemical structures and (b) energy levels of donor molecules (PIPCP, PM2 and PTB7-Th) and acceptor molecules ($PC_{61}BM$, $PC_{71}BM$ and ITIC-Th) investigated for this study.

A collection of the nonradiative recombination loss data collected from a variety of systems using each of the three discussed approaches is shown in Table 1, where "Method 1" refers to the EQE_{EL} measurement, "Method 2" refers to the EQE_{PV}-based calculation, and "Method 3" refers to the simultaneous fitting of CT spectra. I observed that Methods 1 and 3 produce consistent results across all systems within 5%, whereas Method 2 is only accurate within 5% for the PTB7-Th blends. The agreement between Method 2 and the other two methods decreases in systems with a low energetic offset between E_{CT} and E_{opt} (PM2 and PIPCP based systems) due to the large contribution of the singlet absorption in the EQE_{PV} integration. To correctly use Method 2 in this case, we may substitute the measured $EQE_{PV}(E)$

for the Marcus Theory CT state fit to the absorption spectra (shown as the dashed lines in Figure 2). It is worth noting that due to the way these methods are derived this essentially reduces Method 2 to Method 3.

Table 1. Table of ΔV_{nr} values obtained in three ways: (1) EQE_{EL} measurement (2) calculating by integrating EQE_{PV} over the black body emission spectra at room temperature. (3) fitting to the reduced absorption and emission spectra of the blend. The percent error of Methods 2 and 3 with respect to Method 1 are also shown.

ΔV_{nr} values [eV]:	Method 1	Method 2	Method 3	% error from 1-2	% error from 1-3
PIPCP:$PC_{61}BM$	0.280	0.244	0.268	12.46%	4.33%
PM2:$PC_{61}BM$	0.357	0.334	0.374	6.33%	4.64%
PTB7-Th:$PC_{71}BM$ (CB:DPE)	0.425	0.412	0.424	2.96%	0.24%
PTB7-Th:$PC_{71}BM$ (CB)	0.400	0.412	0.418	2.92%	4.52%
PTB7-Th:$PC_{71}BM$ (DCB:DIO)	0.405	0.391	0.410	4.89%	1.30%
PTB7-Th:$PC_{71}BM$ (DCB)	0.399	0.380	0.400	4.59%	0.26%

I conducted the analyses in the remainder of this investigation with the limitations of each method in mind and precisely found the voltage loss breakdown for several blend systems, further analyzing the trends I observed to gain insight into factors which affect the nonradiative voltage loss of an OPV.

B. Impact of structural modifications to donor

To help inform synthetic efforts in making low V_{OC} loss OPV materials, I searched for patterns among specific donor/acceptor units present in the donor polymer and systems which have low nonradiative recombination losses. While I would expect the donor polymer's electron-poor unit to have a larger impact on recombination loss than its electron donating unit, that is not necessarily the case. It is possible that the steric bulk induced by the donor unit of the electron donating material will influence the packing of the blend as a whole, such that the

coupling between the electron donating material and the electron accepting material is less favorable.

The three donor polymers chosen for this investigation are PIPCP, which has the structure "IDT-PT-CPDT-PT", in which IDT=indacenodiphiophene, PT=pyridyl[2,1,3]thiadiazole and CPDT=cyclopentadithiophene, PM2, which has the structure "BDT-PT-CPDT-PT", where BDT=benzodithiophene and the remaining units are shared with PIPCP, and PTB7-Th,[33] which shares the BDT donating unit with PM2.

Wang et. al. reported the synthesis of PM2 as a follow-up to PIPCP; despite the incredibly low voltage losses in the PIPCP:$PC_{61}BM$ system, its performance was plagued by low FF.[12,31,34] The two polymers have the D-A-D-A structure, and share three out of the four structural units: the strong acceptor-strong donor- strong acceptor units "PT-CPDT-PT." The electron-donating BDT unit used in PM2 is much less bulky than the IDT unit of PIPCP, which did result in lower π-π stacking distances (from 4.3 Å to 3.8 Å).[31] PTB7-Th, which also contains the BDT unit, was used as a third point of reference for structural comparisons. Critically, all three of these systems also have very similar E_{CT} values (between 1.38 and 1.45 eV), as shown in **Table 2**.

1. Photovoltaic performance

The optimized conditions for each blend system were used for all device characterization, as taken from literature, and can be found in the Appendix.[12,31,35] **Figure 4** shows the J-V characteristics at 1 sun illumination (100 mW cm^{-2} AM 1.5) for the three fullerene-based blends investigated, where all three blends show comparable device performance to previously published results. The average values have been obtained by testing at least 30 devices each in total from multiple batches. For PIPCP:$PC_{61}BM$ the average PCE

is 5.7%, with a FF of 48±2%, a V_{OC} of 0.900±0.005V and a J_{SC} of 13.2±1 mA cm^{-2}. PM2:$PC_{61}BM$ has an overall higher PCE than PIPCP of 8.0% due to its increased FF and J_{SC} of 61.2±4% and 15.7±1mA cm^{-2}, respectively, but has a significantly lower V_{OC} of 0.806±0.005V. Finally, PTB7-Th:$PC_{71}BM$ has the highest PCE of 9.3% with a V_{OC} comparable to PM2:$PC_{61}BM$ of 0.804±0.002V, and the highest FF and J_{SC} of all three systems of 65.3±2% and 17.7±0.3mA cm^{-2}, respectively.

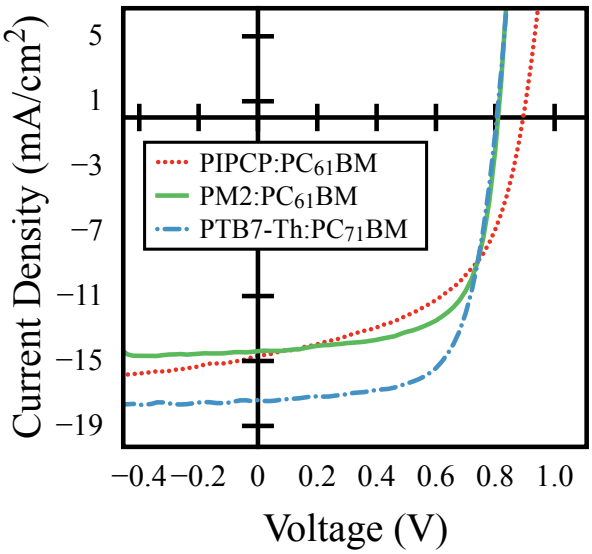

Figure 4. Current density-voltage characteristics of the three optimized fullerene-based blend systems investigated in this study.

2. Light intensity dependence of V_{OC}

I also sought to identify the nature of recombination in these systems. If recombination does not originate from the same mechanism, mono- (trap-assisted) or bimolecular recombination, consideration of the recombination pathways may not be system comparable. I explored the recombination mechanisms by considering the dynamics of carrier density as it relates to the V_{OC}, by first describing V_{OC} using **Equation 13**,[36]

$$V_{OC} = \frac{E_{opt}}{q} - \frac{k_B T}{q} ln\left(\frac{n_e n_h}{N_C^2}\right) \quad (13)$$

Here, the first term describes the basic energetic gap ($E_{LUMO}^{Fullerene} - E_{HOMO}^{Polymer} - \Delta$), where Δ describes the disorder originating from the solution casting of the films, estimated at 0.3 V) and the second term describes the temperature-dependent filling of available conductive states, where n_e and n_h are electron and hole density, respectively, and N_c is the available conductive states in the donor and acceptor, here assumed to be equal. At open circuit conditions no charges are swept out of the device and therefore the recombination rate R is equal to the charge generation rate G as shown in **Equation 14**.[37] Here n_{oc} is charge (either electron or hole) density at open circuit, τ_r is the monomolecular recombination lifetime, and γ is the bimolecular recombination coefficient.[38]

$$R(V_{OC}) = G = \frac{n_{OC}}{\tau_r} + \gamma n_{OC}^2 \quad (14)$$

It can then be understood that the system shall become bimolecular recombination dominant at such a point which $\gamma n_{OC} > 1/\tau_r$, therefore $(n_{OC})^2 = n_e n_h = G/\gamma$. Inserting this into **Equation 14**, we expect to describe change in V_{oc} with incident light intensity I, as $\delta V_{OC} = (k_B T/q)\, ln(I) + constant$. Thus when V_{OC} is plotted as a function of light intensity, we expect to observe a slope of $k_B T/q$;[39] however, if recombination is monomolecular dominant, then both n_e and n_h would be intensity dependent and the slope of the graph would approach $2k_B T/q$.[39,40]

Considering the systems in **Figure 5**, I make several observations. Over the entire intensity range, the slopes vary from 1.08 $k_B T/q$ in the PIPCP system to 1.28 $k_B T/q$ for the PM2 system. This shows that when intensity is considered from 1.0 sun (100 mW cm^{-2} AM 1.5G) to the very low carrier densities present at 0.01 sun, we see the convolution of

monomolecular recombination in these systems most likely from Shockley-Read-Hall (SRH) deep traps.[40] Nevertheless, all these systems appear to be bimolecular dominant in recombination. When the V_{OC} versus ln(light intensity) is examined for the systems at higher light intensities as shown in the **Figure 5 inset**, the PIPCP:$PC_{61}BM$ and PTB7-Th:$PC_{71}BM$ systems converge to a slope of k_BT/q while PM2:$PC_{61}BM$ has a decreased slope of 1.18 k_BT/q. This indicates that at the carrier density produced by ~1 sun illumination, all three systems appear to be bimolecular recombination dominant, making them comparable to one another and viable candidates for the three analyses mentioned above for determining ΔV_{nr}. I confirmed that these varied slopes are not an artifact due to leakage current[41] by examining the light intensity JVs at reverse bias, which can be found in the Appendix.

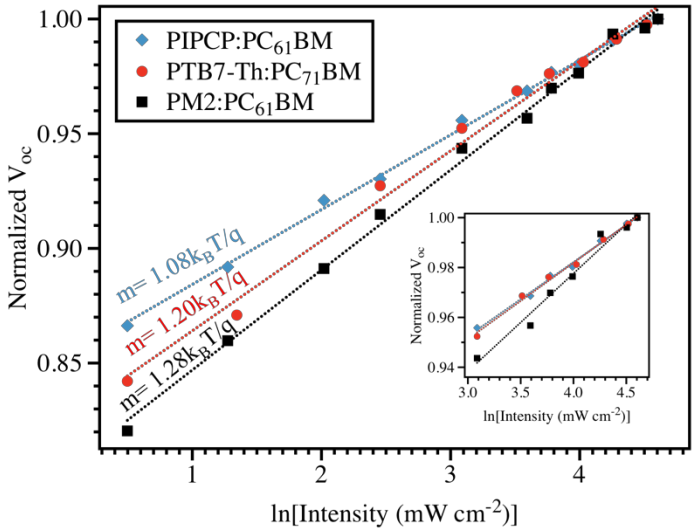

Figure 5. Normalized open-circuit voltage versus the natural log of the illumination intensity for the three optimized, fullerene-based blends. The slopes of the best-fit lines of V_{OC} versus the natural log of illumination intensity relative to k_BT/q are shown. The inset graph shows fits to only the higher light intensity data, for which the slope of the best fit lines for PIPCP:$PC_{61}BM$ and PTB7-Th:$PC_{71}BM$ are approximately k_BT/q and for PM2:$PC_{61}BM$ the slope of the fit line is $1.18k_BT/q$.

2. Impact on nonradiative loss

Upon determining the detailed voltage loss breakdown for these blend systems (**Table 2**) a few things become clear. First, the radiative loss in all three fullerene-based systems remain essentially constant around 0.22-0.21 eV. The nonradiative recombination loss, however, spans a range of 150 meV, despite the similar values of E_{CT}. PIPCP:$PC_{61}BM$ shows the lowest magnitude of nonradiative loss at 0.28 eV, PM2:$PC_{61}BM$ has ΔV_{nr} = 0.37 eV and PTB7-Th:$PC_{71}BM$ has the highest nonradiative loss at 0.43 eV.

To understand why the ΔV_{nr} in these systems vary, I considered the components of the donor polymers. PIPCP, which showed the lowest loss, contains a bulky IDT unit rather than the BDT unit. The rigid conjugation and bulky side chains of the IDT unit perhaps prevent PIPCP from packing as closely to the fullerene molecules as its PM2 counterpart, which might explain the lower nonradiative loss.[42] The PM2 and PTB7-Th systems have a lower open-circuit voltage of 0.8 V as compared to 0.9 V, which can be explained by the higher ΔV_{nr}. As previously mentioned, BDT-based systems tend to have closer packing than IDT systems, resulting in lower π-π stacking distances.[31,43–45] Because one hypothesis is that nonradiative voltage loss is largely due to vibrational energy transfer between donor and acceptor, it is possible that the average physical distance between the molecules in a π-π stack plays a role in this. Of course, a larger data set would need to be studied to better substantiate this hypothesis. Moreover, rushing to implement a design strategy based on maximizing π-π stacking distance will no doubt also affect other properties of the blend that may reduce its effective semiconductor behavior. Nevertheless, these preliminary results suggest there may be a potentially beneficial trade-off to consider.

Table 2. Voltage loss breakdown for each blend system. The optical gap (E_{opt}) was determined by extrapolating from the low energy absorption edge of the blend, and is an estimation of E_g. E_{CT} was found via simultaneous Marcus theory fitting to the EL and EQE_{PV}, where the reciprocity relationship was employed for the PIPCP and PM2 systems which do not have clear CT state shoulder peaks in the measured EQE_{PV}. The fits and fit parameters are shown in Figure S1. ΔV_{rad} was determined from the CT state fits via Equation 11. ΔV_{nr} is found from the EQE_{EL} measurement, and has been verified from fitting to EQE_{PV} to agree within 5 percent. The V_{OC} of the devices was determined via J-V measurements under AM 1.5 illumination.

D:A System	E_{opt} [eV]	E_{CT} [eV]	ΔV_{rad} [eV]	ΔV_{nr} [eV]	qV_{OC} [eV]
PIPCP:$PC_{61}BM$	1.41	1.40	0.22	0.28	0.90
PM2:$PC_{61}BM$	1.43	1.38	0.21	0.37	0.80
PTB7-Th:$PC_{71}BM$	1.58	1.45	0.22	0.43	0.80

C. Impact of changing from fullerene to nonfullerene acceptor

In addition to examining the relationship between the donor polymer and ΔV_{nr} of the system, I also looked into the differences in losses between D:F (donor:fullerene) and D:NF (donor:nonfullerene) blend systems. Several nonfullerene-based blend systems have shown low recombination losses, which can in-part explain the higher performances these systems can achieve over fullerene-based systems.[13,28,46] In my investigation, however, there was not a predictable trend for ΔV_{nr} between the fullerene- and the nonfullerene-based systems. Interestingly though, when the three donors (PIPCP, PM2 and PTB7-Th) were paired with the same non-fullerene acceptor, ITIC-Th, the resulting open-circuit voltage change from that of their fullerene counterparts was also quite variable. The J-V measurements for representative optimized devices of PIPCP:ITIC-Th, PM2:ITIC-Th and PTB7-Th:ITIC-Th under 1 sun illumination can be found in the Appendix, Figure S5. The V_{OC} of the PTB7-Th systems is almost unchanged between D:F and D:NF (0.802±0.004 and 0.804±0.002 V, respectively),

the V_{OC} of PIPCP:ITIC-Th is slightly higher than PIPCP:$PC_{61}BM$ with an improvement of about 30 meV (0.926±0.006 and 0.900±0.005 V), but the PM2:ITIC-Th system shows an increase of 100 meV over the optimized fullerene system (0.899±0.003 and 0.806±0.005 V),.

To understand these differences in V_{OC}, I completed the detailed voltage loss breakdown for each system (see Table S2) and found that the differences can be attributed almost completely to differences in nonradiative loss. For PM2:$PC_{61}BM$, for example, ΔV_{nr} = 0.37 eV, whereas PM2:ITIC-Th shows ΔV_{nr} = 0.28 eV. While this showed that in the case of PM2, the nonradiative voltage loss was greatly diminished in the nonfullerene system, the trend did not carry over to the PIPCP and PTB7-Th systems. The PTB7-Th systems show relatively high loss in both cases and the PIPCP systems both show relatively low ΔV_{nr}. The precise reason for this requires careful consideration, and certainly more exploration. One possible speculation could be that the difference in the strength of D-A interaction is greater between D:F and D:NF for PM2 than for the other two polymer systems.

I also investigated the blend morphology using resonant-soft x-ray scattering measurements (R-SoXS) to better understand the relative domain purity between all six blend systems. By utilizing soft-x-rays which are resonant with the energy of the core-levels of smaller atoms, R-SoXS can achieve greatly enhanced contrast between the donor and the acceptor regions of the film, which consist of either pure material or an intimately mixed blend of the two. The composition variation (or relative domain purity) over the length scales probed can be extracted by integrating scattering profiles to yield the integrated scattering intensity (ISI),[47] in which higher ISI correlates with higher relative domain purity.

The RSoXS profiles for all six blends are shown in **Figure 6A**, and the relative domain purity and center-to-center domain spacing for each individual system are listed in the

Appendix. In general, the PTB7-Th:ITIC-Th based systems showed the highest relative domain purity, along with PM2:$PC_{61}BM$ whereas the PIPCP-based systems and PM2:ITIC-Th show lower domain purity. I further related this information to the ΔV_{nr} for each system, and observed the correlation shown in **Figure 6B**. For the systems I examined, blends with relatively more pure domains had notably higher degrees of ΔV_{nr} than the three systems with lower domain purity.

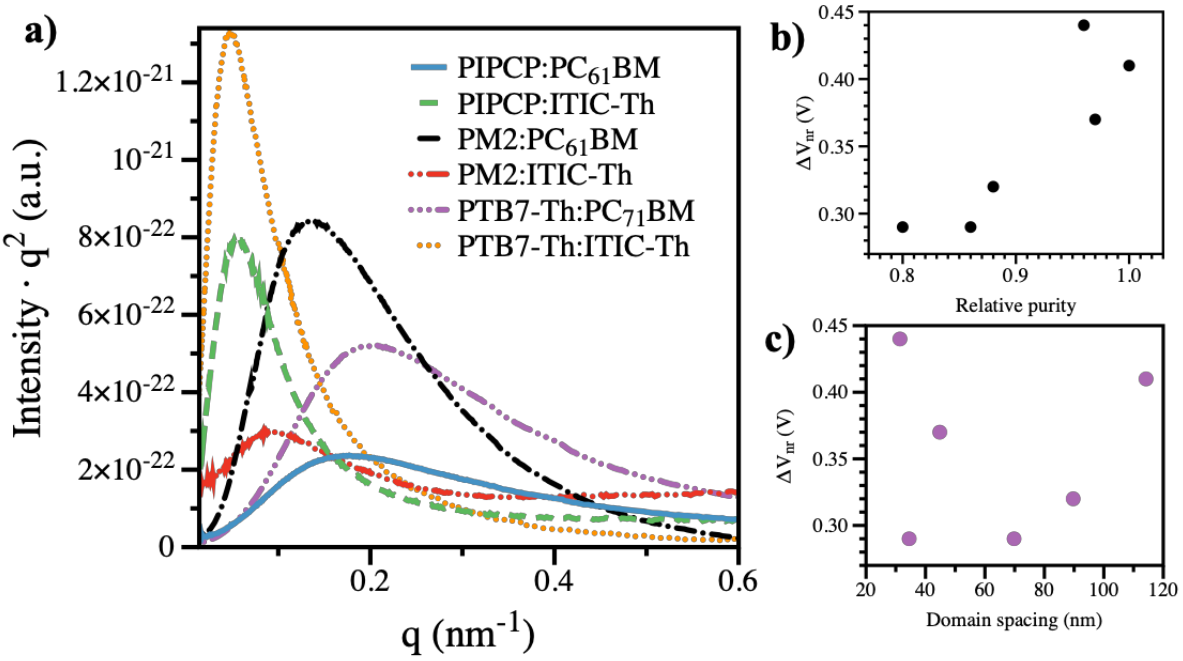

Figure 6. (a) RSoXS profile of the optimized fullerene and nonfullerene-based blend systems (b) ΔV_{nr} as a function of relative purity, based on the ICI values (c) ΔV_{nr} as a function of center-to-center domain spacing.

While this result was initially puzzling, insight can be gained from this correlation. It has been shown by Vandewal et. al. that increasing the donor/acceptor interfacial area leads to increased ΔV_{nr};[48] however, I believe what we are probing has more to do with the nature of those interfaces. It has been shown that there is a tradeoff between domains where the donor and acceptor materials are intimately mixed and regions of pure donor and pure acceptor in achieving high charge generation and low recombination.[49] What may be occurring is that

blends with a higher percentage of pure domains may also have more rigid, crystalline interfaces between donor and acceptor than in systems with a larger proportion of mixed region, where the energy cascade allowed by the mixed regions allows for more efficient energy transfer between donor and acceptor, thus decreasing nonradiative recombination loss.

It is shown in **Figure 6C** that there is no apparent relationship between center-to-center domain spacing and ΔV_{nr}. The ITIC-Th-based blends all showed much higher center-to-center domain spacing than the fullerene-based blends (>90nm compared to <50nm in fullerene blends) which is likely indicative of the large crystalline ITIC-Th domains compared to smaller fullerene domains, rather than suggesting the nonfullerene-based systems also have larger donor domains than fullerene-based blends. Thus, because absorption takes place primarily in the donor material, the large size of ITIC-Th domains does not appear to play a role in increased nonradiative recombination.

C. Impact of changing morphology in PTB7-Th:$PC_{71}BM$ blend

The answer to the question of morphology's impact on ΔV_{nr} has remained somewhat ambiguous in the literature, despite several attempts to gain clarity.[19,20,48] To more generally consider the potential impacts of morphology on nonradiative recombination, I examined PTB7-Th:$PC_{71}BM$, whose morphology has been well-characterized under various solvent conditions, including pure o-dichlorobenzene (DCB) and DCB with 2% (v/v) of the solvent additive 1,8-diiodooctane (DIO).[35] I included two more solvent systems in this study as well, chlorobenzene (CB) and CB with 3% (v/v) diphenylether (DPE), which show evidence of having varying surface topography via atomic force microscopy measurements (**Figure 7A&B**). I chose PTB7-Th:$PC_{71}BM$ specifically because the V_{OC} remains constant despite solvent-based morphology changes (**Figure 7C**), hypothesizing that if nonradiative

recombination is intrinsically changed when the morphology alone is changed, the ratio of nonradiative to radiative loss will increase. **Figure 7D** shows the resulting $EQE_{EL}(V)$ spectra for all four solvent systems, showing that the ΔV_{nr} of the blend stays within 15 meV regardless of solvent, suggesting that changing the morphology via changing the solvent or solvent drying time did not impact the ΔV_{nr} of this blend system. I noted that the pure CB system shows a higher voltage dependence than the other three systems, likely due to traps induced by the large features seen in Figure 7A. Nonetheless, across the entire relevant voltage range it is clearly comparable in magnitude to the other systems, which is confirmed by the determination of ΔV_{nr} via calculation-based methods, as shown in Table 1.

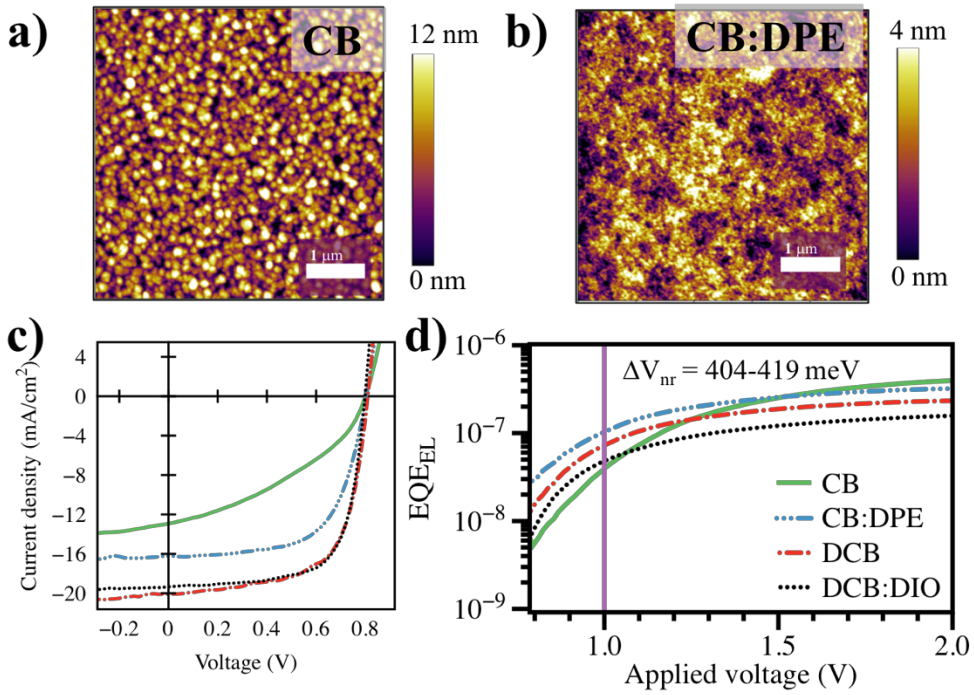

Figure 7. (a) & (b) AFM topography images of PTB7-Th:$PC_{71}BM$ cast from (a) chlorobenzene and b) chlorobenzene with 3% diphenyl ether (c) J-V spectra for representative devices of each of the four conditions, showing varied FF and J_{SC} but the same V_{OC}. d) Measured EQE_{EL} as a function of applied voltage for PTB7-Th:$PC_{71}BM$ cast from chlorobenzene with and without diphenyl ether, as well as from dichlorobenzene and dichlorobenzene with 3 percent DIO. The vertical line represents the approximate voltage at which the injected current is equal to the measured J_{SC} of the devices under illumination (V_{Jsc}) and is thus the point at which ΔV_{nr} was evaluated via Equation 2.

III. Conclusion

In summary, I have provided an in-depth evaluation of the methods used to determine ΔV_{nr} in OPV literature and proposed solutions for problems encountered when measuring ΔV_{nr} in systems with low energetic offsets between E_g and E_{CT}. I suggest using the EQE_{EL} method in conjunction with the fitting or the EQE_{PV}-based calculation to ensure agreement between experimental- and calculation-based methods. I also used several high performing systems with varied ΔV_{nr} to investigate possible relationships between the degree of nonradiative recombination loss and the interaction between donor and acceptor. The primary conclusions from this investigation can be summarized as follows:

(i) In my assessment of fullerene-based systems, PIPCP:$PC_{61}BM$ showed 90 meV less nonradiative recombination loss than PM2:$PC_{61}BM$, resulting in a higher V_{OC} in the PIPCP system. I propose that the steric inhibition induced by bulky groups along the polymer backbone in PIPCP may, in fact, be beneficial for achieving lower ΔV_{nr} due to increased π-π stacking distances and thus less nonradiative energy transfer.

(ii) There is not a predictable change in ΔV_{nr} when switching from fullerene to non-fullerene acceptors, indicating that this value is dictated more by the interactions within a specific donor-acceptor pair than by any particular component. These interactions were probed via RSoXS measurements, which show that systems with higher relative domain purity also exhibit higher nonradiative recombination loss. This result hints that systems with a higher percentage of mixed domains have more favorable interactions between donor and acceptor, resulting in more efficient energy transfer and thus lower vibrational energy loss.

(iii) When morphology changes are induced to the PTB7-Th:$PC_{71}BM$ system using various solvents and additives I still see ΔV_{nr} values within 15 meV, suggesting that altering morphology in this way cannot induce large differences in nonradiative loss.

Overall, I believe delving further into the donor-acceptor coupling and specifics of the donor acceptor interface is necessary to understand and ultimately control this parameter. My work contributes to the body of knowledge within the OPV research community of factors which may affect nonradiative recombination loss and emphasizes once again that ΔV_{nr} is a complex parameter. Continuing to work to understand this elusive loss mechanism is crucial to increasing the open-circuit voltage, and ultimately the efficiency of OPV devices.

IV. Experimental Section

UV-visible absorption spectroscopy: Absorption spectra of neat and blend films were collected using a Perkin Elmer Lambda 750 spectrophotometer. The films were prepared on clean glass slides following the same procedure used for the active layer in the optimized devices.

Device Preparation: ITO patterned glass substrates were thoroughly cleaned by first scrubbing with soapy water, then sonicating in soapy water, deionized water, acetone and isopropyl alcohol, sequentially and dried using compressed nitrogen. ZnO was used as the transparent electrode, where the ZnO solution was prepared in a nitrogen glovebox immediately before spin casting by mixing tetrahydrofuran and diethylzinc (2:1). The fresh ZnO solution was then spun coat atop the clean ITO substrates at 4000 rpm for 30 seconds (PWMSO Series Photo Resist Spinner) then placed on a hotplate at 110 °C for 15 minutes. The active layer of study was spun cast atop the bottom electrode in an inert N_2 environment following the optimized conditions for each blend as listed in the Appendix. All solutions were prepared previously and stirred on a hotplate overnight before casting, and all thermal annealing of the active layer was carried out with substrates directly on the hotplate. The devices were finished by thermal evaporating 7 nm of MoO_x and 100 nm of Ag using the

Angstrom Engineering Series EQ Thermal Evaporator. The device J-V characteristics were measured in a nitrogen-purged glovebox using a Keithley 2602, both in the dark and under simulated 1 sun (100 mW cm^{-2} AM 1.5G) irradiation to assess device leakage and ensure appropriate device performance. The optimized conditions for each blend are given in the Appendix.

Light Intensity Dependent Current-Voltage Measurements: Light intensity dependent J-V measurements were conducted using the same setup as the 1 sun illumination, with filters of various optical densities placed in front of the light source. The exact power density was calibrated for each filter using the Keithley 2602 immediately before conducting measurements.

EQE_{PV} Measurements: Photovoltaic external quantum efficiency was measured in a nitrogen-purged glovebox using a setup which consisted of a 75 W Xe lamp, monochromator, optical chopper and a lock-in amplifier. A National Institute of Standards and Technology calibrated silicon photodiode was used for calibration.

Electroluminescence and EQE_{EL} Measurements: The EL spectra for each blend was obtained by applying a small bias (such that the measured current is close to the device's J_{SC} under 1 sun illumination) to the optimized solar cell. The resulting emission was collected using an Andor SR393i-B spectrometer with a cooled silicon detector DU420ABR-DD, and was corrected for detector response using the spectra from a blackbody emitter placed under the same optics.

The efficiency of the electroluminescence was obtained by applying a bias to the solar cell and placing a 1 cm^2 silicon photodiode directly in front of it to collect the resulting emission. This was accomplished using a dual-channel Keithley 2602 to sweep a small bias

across the solar cell and simultaneously measure the current through the OPV and through the photodiode. The number of photons emitted per electron injected can then be calculated using the EL spectra of the device and the sensitivity of the photodiode, the details of which can be found in the Appendix. All systems measured in this way were checked using multiple devices on multiple days, at various distances (4 cm and <1 cm) and at different angles between OPV and photodiode to ensure the robustness of the measurement (**Figure S4)**.

Atomic Force Microscopy: AFM measurements were performed with an Asylum Research MFP-3D microscope sitting atop an inverted optical microscope (Olympus, IX71). All measurements were done under inert atmosphere. Chromium/platinum-coated silicon probes with a spring constant of 0.2 N m^{-2} and resonant frequency of 13 kHz (Budget Sensors) were used in contact-mode operation.

Resonant Soft X-ray Scattering Characterization: R-SoXS transmission measurements were performed at beamline 11.0.1.2[9] at the ALS. Samples for R-SoXS measurements were prepared on a PSS modified Si substrate under the same conditions as those used for device fabrication, and then transferred by floating in water to a 1.5×1.5 mm, 100 nm thick Si_3N_4 membrane supported by a 5×5 mm, 200 mm thick Si frame (Norcada Inc.). Two- dimensional scattering patterns were collected on an in-vacuum CCD camera (Princeton Instrument PI-MTE).

References

[1] G. A. dos Reis Benatto, M. Corazza, B. Roth, F. Schütte, M. Rengenstein, S. A. Gevorgyan, F. C. Krebs, *Energy Technology* **2017**, *5*, 338.

[2] Y.-J. Heo, Y.-S. Jung, K. Hwang, J.-E. Kim, J.-S. Yeo, S. Lee, Y.-J. Jeon, D. Lee, D.-Y. Kim, *ACS Appl. Mater. Interfaces* **2017**, *9*, 39519.

[3] D. Chemisana, A. Moreno, M. Polo, C. Aranda, A. Riverola, E. Ortega, C. Lamnatou, A. Domènech, G. Blanco, A. Cot, *Renewable Energy* **2018**, DOI 10.1016/j.renene.2018.03.073.

[4] J. Yuan, Y. Zhang, L. Zhou, G. Zhang, H.-L. Yip, T.-K. Lau, X. Lu, C. Zhu, H. Peng, P. A. Johnson, M. Leclerc, Y. Cao, J. Ulanski, Y. Li, Y. Zou, *Joule* **2019**, DOI https://doi.org/10.1016/j.joule.2019.01.004.

[5] S Li, L. Ye, W. Zhao, H. Yan, B. Yang, D. Liu, W. Li, H. Ade, J. Hou, *Journal of the American Chemical Society* **2018**, *140*, 7159.

[6] W. Zhao, S. Li, H. Yao, S. Zhang, Y. Zhang, B. Yang, J. Hou, *Journal of the American Chemical Society* **2017**, *139*, 7148.

[7] X. Guo, N. Zhou, S. J. Lou, J. Smith, D. B. Tice, J. W. Hennek, R. P. Ortiz, J. T. L. Navarrete, S. Li, J. Strzalka, L. X. Chen, R. P. H. Chang, A. Facchetti, T. J. Marks, *Nature Photonics* **2013**, *7*, 825.

[8] Y. Liu, J. Zhao, Z. Li, C. Mu, W. Ma, H. Hu, K. Jiang, H. Lin, H. Ade, H. Yan, *Nature Communications* **2014**, *5*, 5293.

[9] J. Benduhn, K. Tvingstedt, F. Piersimoni, S. Ullbrich, Y. Fan, M. Tropiano, K. A. McGarry, O. Zeika, M. K. Riede, C. J. Douglas, S. Barlow, S. R. Marder, D. Neher, D. Spoltore, K. Vandewal, *Nature Energy* **2017**, *2*, 17053.

[10] D. Baran, T. Kirchartz, S. Wheeler, S. Dimitrov, M. Abdelsamie, J. Gorman, R. S. Ashraf, S. Holliday, A. Wadsworth, N. Gasparini, P. Kaienburg, H. Yan, A. Amassian, C. J. Brabec, J. R. Durrant, I. McCulloch, *Energy Environ. Sci.* **2016**, *9*, 3783.

[11] K. Vandewal, J. Benduhn, V. C. Nikolis, *Sustainable Energy & Fuels* **2018**, *2*, 538.

[12] N. A. Ran, J. A. Love, C. J. Takacs, A. Sadhanala, J. K. Beavers, S. D. Collins, Y. Huang, M. Wang, R. H. Friend, G. C. Bazan, T.-Q. Nguyen, *Adv. Mater.* **2016**, *28*, 1482.

[13] S. Chen, Y. Wang, L. Zhang, J. Zhao, Y. Chen, D. Zhu, H. Yao, G. Zhang, W. Ma, R. H. Friend, P. C. Y. Chow, F. Gao, H. Yan, *Advanced Materials* **2018**, *30*, 1804215.

[14] U. Rau, *Phys. Rev. B* **2007**, *76*, 085303.

[15] K. Vandewal, K. Tvingstedt, A. Gadisa, O. Inganäs, J. V. Manca, *Phys. Rev. B* **2010**, *81*, 125204.

[16] K. Vandewal, K. Tvingstedt, A. Gadisa, O. Inganäs, J. V. Manca, *Nature Materials* **2009**, *8*, 904.

[17] N. A. Ran, S. Roland, J. A. Love, V. Savikhin, C. J. Takacs, Y.-T. Fu, H. Li, V. Coropceanu, X. Liu, J.-L. Brédas, G. C. Bazan, M. F. Toney, D. Neher, T.-Q. Nguyen, *Nature Communications* **2017**, *8*, 79.

[18] D. Baran, M. S. Vezie, N. Gasparini, F. Deledalle, J. Yao, B. C. Schroeder, H. Bronstein, T. Ameri, T. Kirchartz, I. McCulloch, J. Nelson, C. J. Brabec, *J. Phys. Chem. C* **2015**, *119*, 19668.

[19] Z. Tang, J. Wang, A. Melianas, Y. Wu, R. Kroon, W. Li, W. Ma, M. R. Andersson, Z. Ma, W. Cai, W. Tress, O. Inganäs, *J. Mater. Chem. A* **2018**, *6*, 12574.

[20] S. M. Tuladhar, M. Azzouzi, F. Delval, J. Yao, A. A. Y. Guilbert, T. Kirchartz, N. F. Montcada, R. Dominguez, F. Langa, E. Palomares, J. Nelson, *ACS Energy Lett.* **2016**, *1*, 302.

[21] J. Liu, S. Chen, D. Qian, B. Gautam, G. Yang, J. Zhao, J. Bergqvist, F. Zhang, W. Ma, H. Ade, O. Inganäs, K. Gundogdu, F. Gao, H. Yan, *Nature Energy* **2016**, *1*, 16089.

[22] X.-K. Chen, M. K. Ravva, H. Li, S. M. Ryno, J.-L. Brédas, *Adv. Energy Mater.* **2016**, *6*, n/a.

[23] X.-K. Chen, J.-L. Brédas, *Advanced Energy Materials* **2018**, *8*, 1702227.

[24] U. Rau, U. W. Paetzold, T. Kirchartz, *Phys. Rev. B* **2014**, *90*, 035211.

[25] M. Kuik, L. J. A. Koster, G. A. H. Wetzelaer, P. W. M. Blom, *Phys. Rev. Lett.* **2011**, *107*, 256805.

[26] G.-J. A. H. Wetzelaer, M. Scheepers, A. M. Sempere, C. Momblona, J. Ávila, H. J. Bolink, *Adv. Mater.* **2015**, *27*, 1837.

[27] J. Yao, T. Kirchartz, M. S. Vezie, M. A. Faist, W. Gong, Z. He, H. Wu, J. Troughton, T. Watson, D. Bryant, J. Nelson, *Phys. Rev. Applied* **2015**, *4*, 014020.

[28] A. Mishra, M. L. Keshtov, A. Looser, R. Singhal, M. Stolte, F. Würthner, P. Bäuerle, G. D. Sharma, *Journal of Materials Chemistry A* **2017**, *5*, 14887.

[29] K. Vandewal, *Semiconductors and Semimetals* **2011**, *85*, 261.

[30] M. Wang, H. Wang, T. Yokoyama, X. Liu, Y. Huang, Y. Zhang, T.-Q. Nguyen, S. Aramaki, G. C. Bazan, *J. Am. Chem. Soc.* **2014**, *136*, 12576.

[31] M. Wang, Hengbin Wang, M. Ford, J. Yuan, C.-K. Mai, S. Fronk, G. C. Bazan, *J. Mater. Chem. A* **2016**, *4*, 15232.

[32] S.-H. Liao, H.-J. Jhuo, Y.-S. Cheng, S.-A. Chen, *Adv. Mater.* **2013**, *25*, 4766.

[33] Y. Lin, F. Zhao, Q. He, L. Huo, Y. Wu, T. C. Parker, W. Ma, Y. Sun, C. Wang, D. Zhu, A. J. Heeger, S. R. Marder, X. Zhan, *J. Am. Chem. Soc.* **2016**, *138*, 4955.

[34] N. A. Ran, J. A. Love, M. C. Heiber, X. Jiao, M. P. Hughes, A. Karki, M. Wang, V. V. Brus, H. Wang, D. Neher, H. Ade, G. C. Bazan, T.-Q. Nguyen, *Adv. Energy Mater.* **2018**, *8*

[35] H. Zhong, L. Ye, J.-Y. Chen, S. B. Jo, C.-C. Chueh, J. H. Carpenter, H. Ade, A. K.-Y. Jen, *J. Mater. Chem. A* **2017**, *5*, 10517.

[36] P. W. M. Blom, V. D. Mihailetchi, L. J. A. Koster, D. E. Markov, *Advanced Materials* **2007**, *19*, 1551.

[37] S. R. Cowan, A. Roy, A. J. Heeger, *Phys. Rev. B* **2010**, *82*, 245207.

[38] G. Garcia-Belmonte, J. Bisquert, *Appl. Phys. Lett.* **2010**, *96*, 113301.

[39] L. J. A. Koster, V. D. Mihailetchi, R. Ramaker, P. W. M. Blom, *Appl. Phys. Lett.* **2005**, *86*, 123509.

[40] V. V. Brus, C. M. Proctor, N. A. Ran, T.-Q. Nguyen, *Advanced Energy Materials* **2016**, *6*, 1502250.

[41] C. M. Proctor, T.-Q. Nguyen, *Appl. Phys. Lett.* **2015**, *106*, 083301.

[42] K. R. Graham, C. Cabanetos, J. P. Jahnke, M. N. Idso, A. El Labban, G. O. Ngongang Ndjawa, T. Heumueller, K. Vandewal, A. Salleo, B. F. Chmelka, A. Amassian, P. M. Beaujuge, M. D. McGehee, *J. Am. Chem. Soc.* **2014**, *136*, 9608.

[43] W. Zhang, J. Smith, S. E. Watkins, R. Gysel, M. McGehee, A. Salleo, J. Kirkpatrick, S. Ashraf, T. Anthopoulos, M. Heeney, I. McCulloch, *J. Am. Chem. Soc.* **2010**, *132*, 11437.

[44] I. McCulloch, R. S. Ashraf, L. Biniek, H. Bronstein, C. Combe, J. E. Donaghey, D. I. James, C. B. Nielsen, B. C. Schroeder, W. Zhang, *Acc. Chem. Res.* **2012**, *45*, 714.

[45] J.-S. Wu, S.-W. Cheng, Y.-J. Cheng, C.-S. Hsu, *Chem. Soc. Rev.* **2015**, *44*, 1113.

[46] W. Zhao, D. Qian, S. Zhang, S. Li, O. Inganäs, F. Gao, J. Hou, *Advanced Materials* **2016**, *28*, 4734.

[47] S. Swaraj, C. Wang, H. Yan, B. Watts, J. Lüning, C. R. McNeill, H. Ade, *Nano Lett.* **2010**, *10*, 2863.

[48] K. Vandewal, J. Widmer, T. Heumueller, C. J. Brabec, M. D. McGehee, K. Leo, M. Riede, A. Salleo, *Adv. Mater.* **2014**, *26*, 3839.

[49] C. Zhong, J. A. Bartelt, M. D. McGehee, D. Cao, F. Huang, Y. Cao, A. J. Heeger, *J. Phys. Chem. C* **2015**, *119*, 26889.

Appendix

The following information serves as a supplement to the body of the M.S.

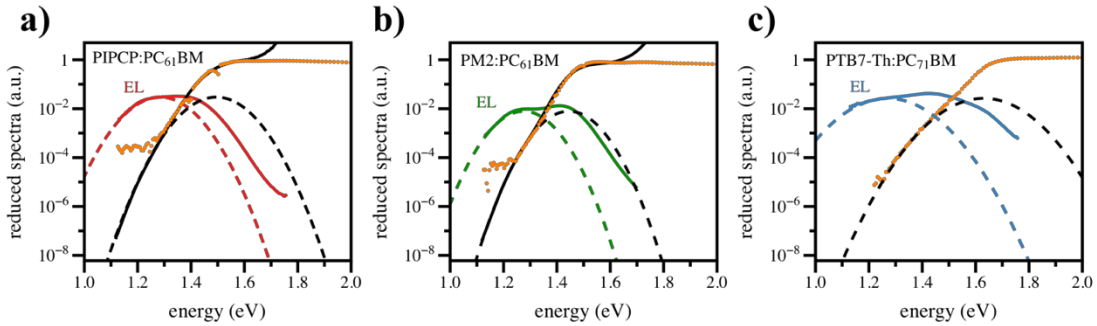

Figure S1. Reduced emission and absorption spectra for the three studied blends with their corresponding Marcus Theory fits. The solid colored lines are the measured electroluminescence spectra for each blend, the orange points are the measured EQE_{PV} spectra and the solid black line is the EQE_{PV} spectrum calculated via the reciprocity relationship between absorption and emission, using equation (x), which shows excellent agreement with the measured points. The dotted lines are the fits to the reduced spectra, calculated from equations (x and y) which were used to determine E_{CT} and $\Delta V_{rad.}$ (a) PIPCP:$PC_{61}BM$, $\lambda = 0.10$ eV, $E_{CT} = 1.390$ eV, $f = 5.50 \times 10^{-3}$ eV^2. (b) PM2:$PC_{61}BM$, $\lambda = 0.090$ eV, $E_{CT} = 1.375$ eV, $f = 2.50 \times 10^{-3}$ eV^2. (c) PTB7-Th:$PC_{71}BM$, $\lambda = 0.18$ eV, $E_{CT} = 1.450$ eV, $f = 7.50 \times 10^{-3}$ eV^2. T= 300K for all fits.

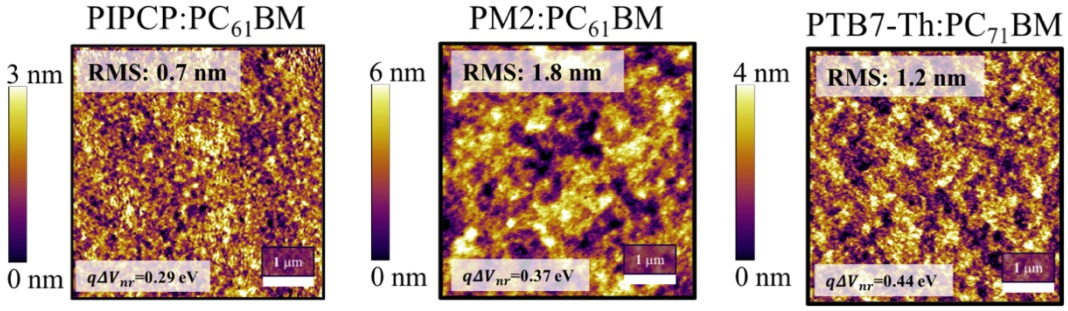

Figure S2. Atomic force microscopy (AFM) topography images of the three optimized blends, showing comparable surface topography and roughness values (RMS) for all three blends.

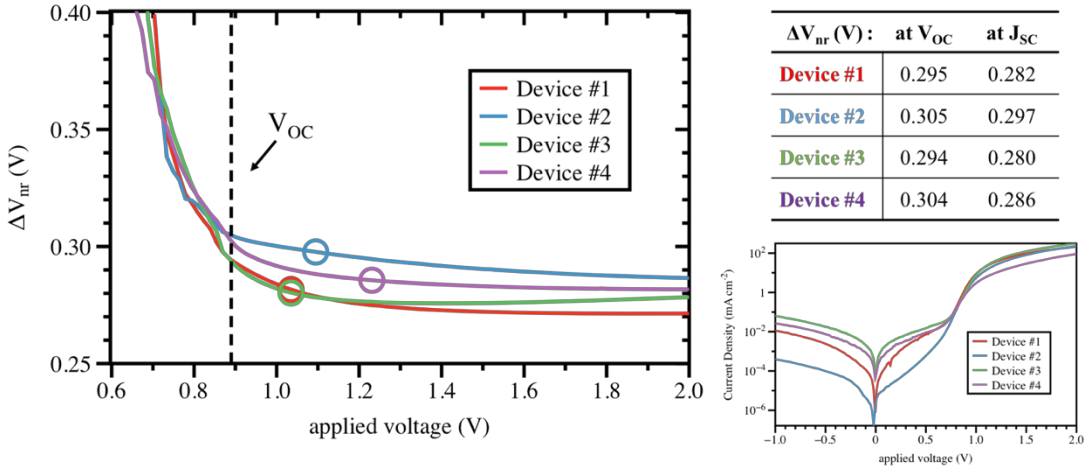

ΔV_{nr} (V) :	at V_{OC}	at J_{SC}
Device #1	0.295	0.282
Device #2	0.305	0.297
Device #3	0.294	0.280
Device #4	0.304	0.286

Figure S3. (on the left) Nonradiative loss as a function of applied voltage for multiple devices of PIPCP:$PC_{61}BM$, which were both prepared and measured on four different days. The dotted vertical line is the applied voltage corresponding to the V_{OC} of the optimized PIPCP:$PC_{61}BM$ devices, and the open circle is the point where the injected current at this applied voltage is equal to the J_{SC} of the device under 1 sun illumination. The table on the top right shows that the difference between these two points is at maximum, less than 20 meV. The small difference in magnitude of ΔV_{nr} for different devices can be understood by observing the difference in the leakage current for each device, shown in the dark JV spectra on the bottom right. The devices with higher leakage current (#1, #3, #4) will have more additional free carriers in the device recombining radiatively, creating a slightly elevated value of EQE_{EL} and thus a slightly lower ΔV_{nr} than in the low leakage device (#2).

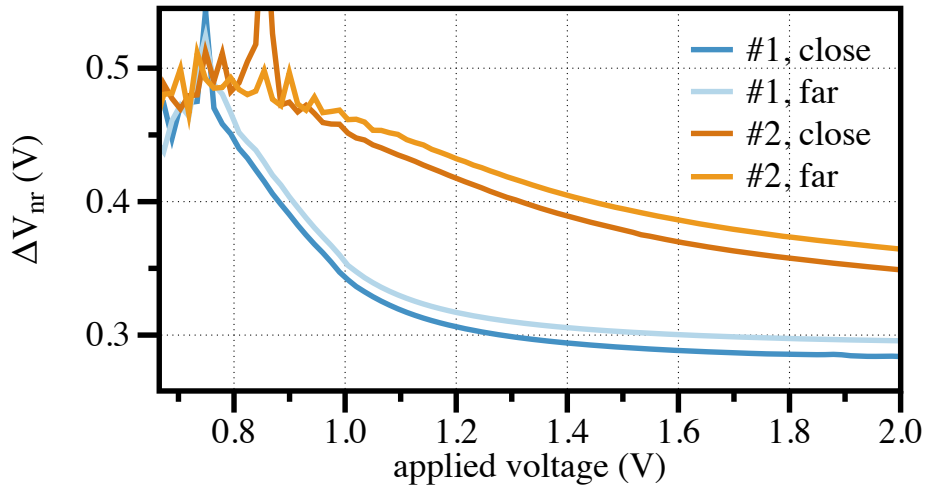

Figure S4. ΔV_{nr} as a function of voltage for a higher loss system (#1) and lower loss system (#2) at two distances from the photodiode, where "close" is less than 1 cm, and well within the range where we can expect almost all photons to reach the photodiode, and "far" is 2 cm, where some photons are expected to scatter outside of the range of the photodiode area. In

both cases the "close" curve can be replicated by the "far" curve by multiplying by a factor of 0.966.

Supplementary Equations and Information for EQE_{EL} Measurement

As explained in Section 2.2.1, the EQE_{EL} is the ratio of photons emitted from the device per electron injected into the device. To correct the photodiode current output from the EQE_{EL} measurement, I_{PD}, for the electroluminescent output of the device to determine number of photons emitted, I_0, we describe I_{PD} as

$$I_{PD} = I_0 \int_{\lambda_1}^{\lambda_2} i(\lambda)s(\lambda)d\lambda \quad \text{(S1)},$$

where the photodiode current is equal to the number of photons scaled by the integration term, where $i(\lambda)$ represents the shape of the device emission spectra such that $i(\lambda)$ integrated over the wavelength range of emission is equal to 1, and $s(\lambda)$ is the sensitivity spectrum of the photodiode. The EQE_{EL} at a given voltage can then be described as I_0 divided by the OPV dark current at the same voltage, I_{OPV},

$$EQE_{EL} = \frac{I_0}{I_{OPV}} \quad \text{(S2)}$$

And by substituting equation S1 into equation S2, we have an equation for EQE_{EL} which is defined in measurable terms.

$$EQE_{EL} = \frac{I_{PD}}{I_{OPV} \int_{\lambda_1}^{\lambda_2} i(\lambda)s(\lambda)d\lambda} \quad \text{(S3)}$$

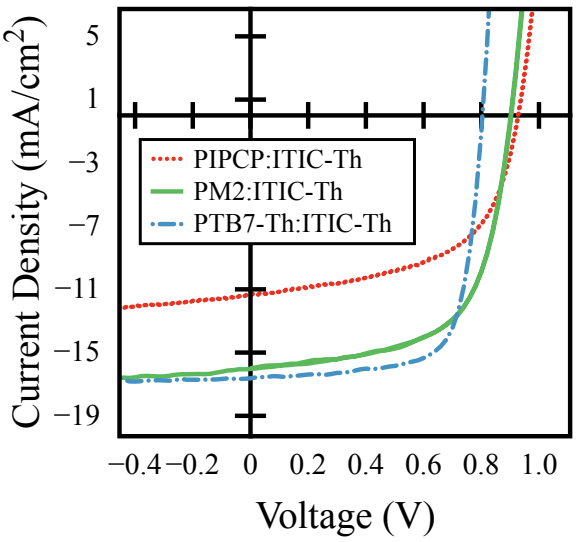

Figure S5. Current density plot of representative devices for the optimized nonfullerene-based blends with PIPCP, PM2 and PTB7-Th.

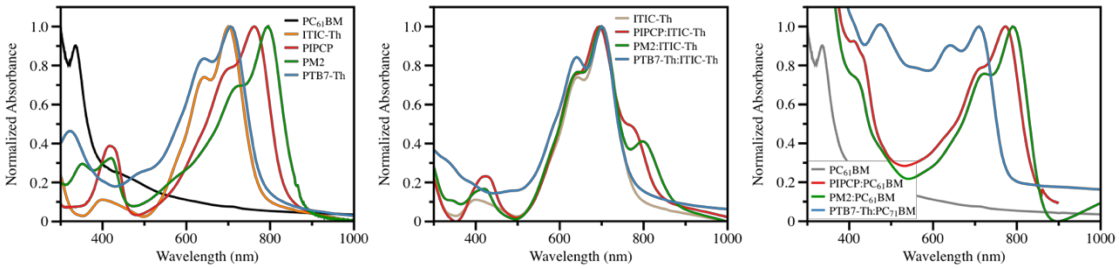

Figure S6. Absorbance profiles for (a) neat materials and (b) fullerene-based blends and (c) nonfullerene-based blends.

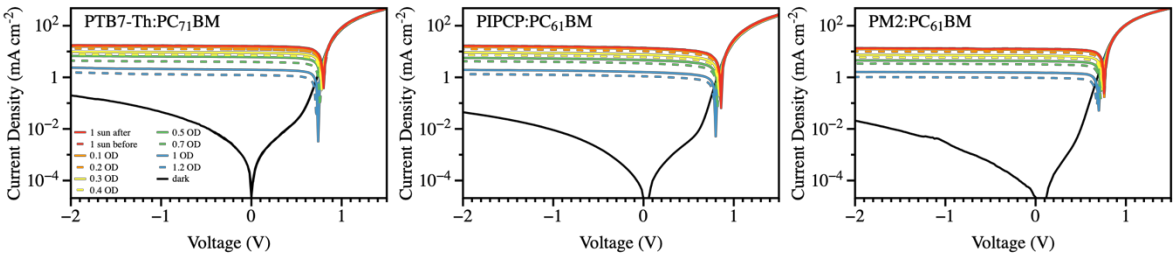

Figure S7. Light intensity JV scans for the three blends examined in Section II.B.2, showing no influence of leakage current

Table S1. Blend conditions for all studied systems.

Material system	Blend Ratio	Concentration (total)	Solvent	Spin Speed	Anneal
PIPCP:$PC_{61}BM$	1:2	20 mg/mL	CF:CB (3:2)	2000 rpm	-
PIPCP:ITIC-Th	1:2	15 mg/mL	CF:CB (3:2)	3000 rpm	80˚C
PM2:$PC_{61}BM$	1:2	20 mg/mL	CB:2%DIO	1200 rpm	80˚C
PM2:ITIC-Th	1:1.5	15 mg/mL	CF:CB (3:2)	3000 rpm	100˚C
PTB7-Th:$PC_{71}BM$ (CB:DPE)	1:1.5	30 mg/mL	CB:3%DPE	1500 rpm	100˚C
PTB7-Th:$PC_{71}BM$ (CB)	1:1.5	30 mg/mL	CB	1500 rpm	100˚C
PTB7-Th:$PC_{71}BM$ (DCB:DIO)	1:1.5	25 mg/mL	DCB:3%DIO	1000 rpm	-
PTB7-Th:$PC_{71}BM$ (DCB)	1:1.5	25 mg/mL	DCB	1000 rpm	-
PTB7-Th:ITIC-Th	1:1.5	25 mg/mL	CF:CB (3:2)	1500 rpm	100˚C

Table S2. ΔV_{nr}, relative purity and domain size information for optimized blend systems. ΔV_{nr} was obtained via EQE_{EL} measurements, and domain size and relative purity were found using R-SoXS.

Material system	E_{opt} (eV)	E_{CT} (eV)	ΔV_{rad} (eV)	ΔV_{nr} (eV)	Relative purity	Center-to-center domain spacing (nm)
PIPCP:$PC_{61}BM$	1.41	1.40	0.22	0.28	0.80	34.5
PIPCP:ITIC-Th	1.48	1.47	0.23	0.31	0.88	89.7
PM2:$PC_{61}BM$	1.43	1.38	0.23	0.35	0.97	44.8
PM2:ITIC-Th	1.44	1.38	0.20	0.28	0.86	89.7
PTB7-Th:$PC_{71}BM$ (CB:DPE)	1.58	1.45	0.22	0.42	0.96	31.4
PTB7-Th:ITIC-Th	1.59	1.39	0.19	0.40	1	114.2